Volume 3 | Number 11 | November 2016

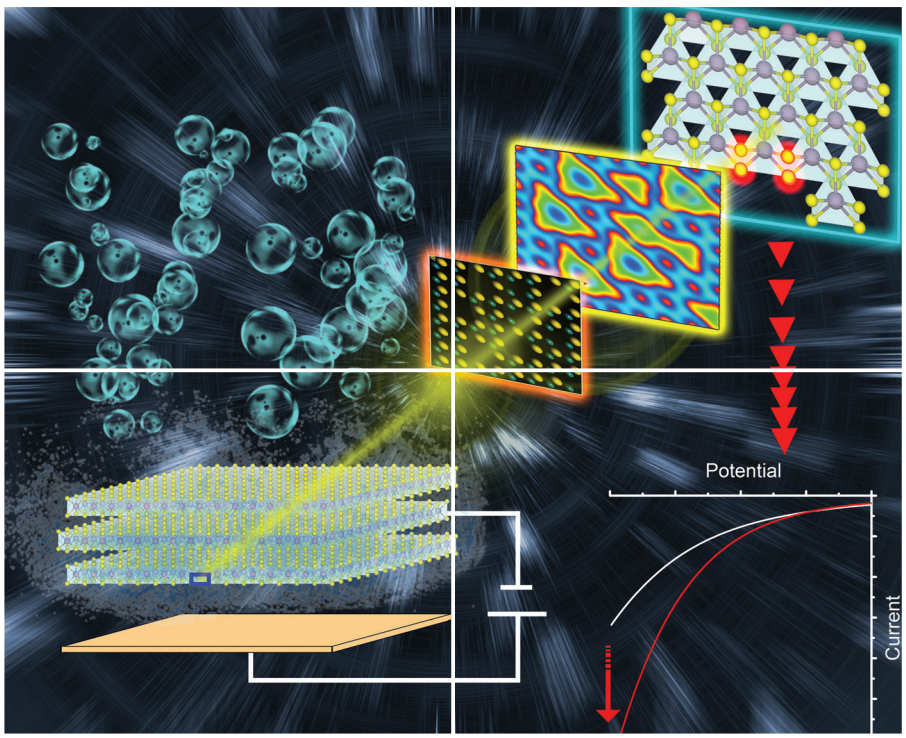

INORGANIC CHEMISTRY

FRONTIERS

Chinese Chemical Society
PEKING UNIVERSITY 1898
ROYAL SOCIETY OF CHEMISTRY

http://rsc.li/frontiers-inorganic

INORGANIC CHEMISTRY
FRONTIERS

RESEARCH ARTICLE

View Article Online
View Journal | View Issue

Cite this: *Inorg. Chem. Front.*, 2016, **3**, 1376

Engineering active sites of two-dimensional MoS_2 nanosheets for improving hydrogen evolution†

Xiangkai Kong,‡[a,b,c] Xiaochen Shen,‡[a] Changlin Zhang,[a] Shirin Norooz Oliaee[a] and Zhenmeng Peng*[a]

Received 24th August 2016,
Accepted 22nd September 2016

DOI: 10.1039/c6qi00334f

rsc.li/frontiers-inorganic

Generating more and fresh active sites is challenging for 2D MoS_2. Herein, the old S edges were peeled off and the inner S atoms were disclosed as under-coordinated atoms. This realized more and freshly active sites being exposed that facilitate adsorption of intermediates and lead to dramatic enhancements in its HER activity in both acid and alkaline electrolytes.

Water electrolysis for generating hydrogen, preferably driven by solar irradiation, is one of the most remarkable methods among all hydrogen production technologies.[1–7] This process is environmentally benign and can be an efficient aid for good electrocatalysts for both hydrogen evolution reaction (HER) and oxygen evolution reaction (OER). Among several developed HER catalysts, noble metals, in particular platinum, are the most active. However, their scarcity and high cost largely limit their practical applicability.[8–10] Hence, identifying and developing high-performance HER electrocatalysts using low-cost and earth-abundant materials remains an urgent requirement.[11,12]

During the past few decades, MoS_2-based structures have been intensively studied for HER behavior and showed promising catalytic properties in the reaction.[13–19] Similar to the graphene structure, the sandwich-like S–Mo–S layers serve as building blocks and stack on each other *via* weak van der Waals interactions, forming layered hexagonally packed structures.[20–23] Both experimental and computational studies discover that the HER activity stems from the S edges of the MoS_2 nanostructure, whereas their basal planes are catalytically inert.[12,24–28] This means the defected sulfur atom sites play a crucial role in the hydrogen evolution process. Thus, designing and engineering nanosized MoS_2 with efficiently exposed under-coordinated S sites should be an effective means to obtain high-performance HER electrocatalysts. Recently, Jaramillo and his colleagues successfully designed and prepared a 3D mesoporous double gyroid MoS_2 thin film based on a Si template with high surface curvature to preferentially expose more active sites.[12] Cui *et al.* used electron beam evaporation to prepare a vertically aligned layered MoS_2 film, which maximizes the exposure of edges on the film surface.[25] Chang's group reported a molecule that mimics the structure of active edge site fragments of MoS_2[27] and Kibsgaard *et al.* demonstrated a similar Mo–S molecular HER catalyst.[28] However, their manipulations were complex and the yields were low, which limited their practical application on a large scale.

Two-dimensional (2D) MoS_2 nanosheets have been extensively investigated for HER due to their unique structure and extremely high surface area.[29,30] Unfortunately, pristine 2D MoS_2 structures exhibit poor catalytic activity. This is caused by the fact that under-coordinated S atoms exist primarily only at edges, with few in surface planes and thus cause a low active site content. Therefore, engineering of more actives sites exposed on the surface of MoS_2 nanosheets is expected to dramatically improve their electrocatalytic HER performance. Nonetheless, rational and controllable active site modulation is still limited.

In the present study, we demonstrated controllable generation of active sites on 2D MoS_2 nanosheets using a simple but robust strategy. As illustrated in Scheme 1, the pristine 2D MoS_2 had two active S sites at edges in the marked area. After exploring, the old Mo atoms and two S atoms were removed or vaporized, facilitating more and fresh inner active S sites exposed to the reactants. The new obtained MoS_2 retained the 2D structure, possessing more density of under-coordinated S atoms and exhibited significantly improved HER activity compared to the pristine counterparts in both acidic and alkaline electrolytes.

The ultrathin MoS_2 nanosheets were synthesized with a hydrothermal method and a post-synthesis annealing treat-

[a]*Department of Chemical and Biomolecular Engineering, University of Akron, Akron, Ohio 44325, USA. E-mail: zpeng@uakron.edu*
[b]*School of Physics and Electronic Information, Huaibei Normal University, Huaibei, Anhui 235000, P. R. China*
[c]*High Magnetic Field Laboratory, Chinese Academy of Science, Hefei, Anhui 230031, P. R. China*

†Electronic supplementary information (ESI) available: Details of Experimental section and electrochemical tests. See DOI: 10.1039/c6qi00334f

‡These authors contributed equally to this work.

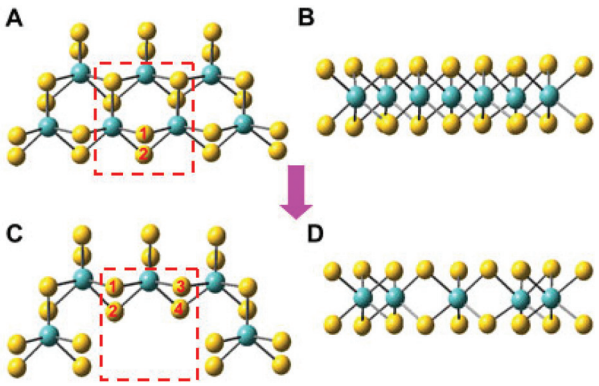

Scheme 1 (A, B) Structural edge model of pristine MoS_2 nanosheets on top and in side view. (C, D) Structural model of annealed MoS_2 nanosheets with more exposed active sties on top and in side view. The blue and yellow balls stand for Mo and S atoms, respectively. All the exposed under-coordinated S atoms have been marked in the selected rectangular area.

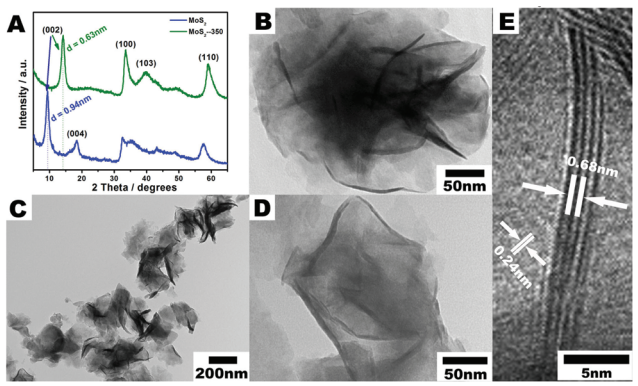

Fig. 1 (A) XRD of pristine MoS_2 and MoS_2-350 nanosheets, (B) TEM of pristine MoS_2, and (C-E) TEM and HRTEM of MoS_2-350.

ment in an Ar atmosphere was then applied. The resultant materials were denoted as MoS_2-XXX, where XXX stands for the annealing temperature. Fig. 1A shows X-ray diffraction (XRD) patterns of both the pristine and the thermo-treated MoS_2. The diffraction pattern of the pristine sample matched well with reference MoS_2 in the 2H phase (JCPDS card no. 73-1508), and it was largely maintained for the MoS_2-350, suggesting the 2H phase is not affected by the post-synthesis treatment and is thermally stable. Moreover, a positive shift in the (002) peak was observed, corresponding to reduced *d*-spacing between this group of planes and is likely associated with removal of moisture between the S–Mo–S layers during the annealing treatment. In addition, the diffraction peaks got sharper and narrower, particularly for the (100) pattern. This suggested that the side edge of the (100) plane, as shown in Scheme 1B, had changed considerably, as well as the crystallinity had increased. Fig. 1B shows a representative transmission electron microscope (TEM) image of the pristine MoS_2 nanosheets. Some ripples and corrugations could be observed, demonstrating the ultrathin nature of the nanosheets. No significant changes in the nanosheet morphology and thickness were observed for the MoS_2 after annealing treatment (Fig. 1C and D), indicating good thermal stability of the layered structure. High resolution TEM (HRTEM) characterization of the vertically aligned nanosheets revealed hexagonal atomic lattices and curled open edges (Fig. 1E). The inter-layer spacing was measured to be 0.68 nm, which was consistent with the XRD result and could be indexed to the (002) planes of 2H-MoS_2. The nanosheet had only five MoS_2 layers, confirming the 2D characteristics. The in-plane lattice spacing was measured to be 0.24 nm, corresponding to the (101) planes of 2H-MoS_2.

The MoS_2 samples were characterized using Fourier transform infrared (FTIR) spectroscopy with no characteristic peaks of thiourea and its derivatives being observed (Fig. 2A), indicating that the organic species could be completely removed from the 2D MoS_2 and the nanosheets have clean surfaces, which is essential for their use as HER catalysts.[31] The Raman spectrum of the pristine MoS_2 showed two peaks located at 377 cm^{-1} and 404 cm^{-1}, which could be assigned to the in-plane E_{2g} and out-of-plane A_{1g} vibrational modes in 2H MoS_2, respectively (seen in Fig. 2B).[32] Slight red shifts were observed for both peaks of the MoS_2 after annealing treatment, implying influence of the thermal treatment on the active sties. The distance between the two peaks remained unchanged, suggesting little change in the thickness of the nanosheets, which is consistent with the TEM observations. Moreover, there was a significant increase of the relative intensity between the two peaks, E_{2g}/A_{1g}, from 1.27 to 1.53, demonstrating the presence of more in-plane defect structures after the annealing treatment. In addition, the surface area after 350 °C treatment had increased from 15.8 to 20.0 $m^2\ g^{-1}$ as measured by N_2 adsorption, confirming the new surface edge exploration.

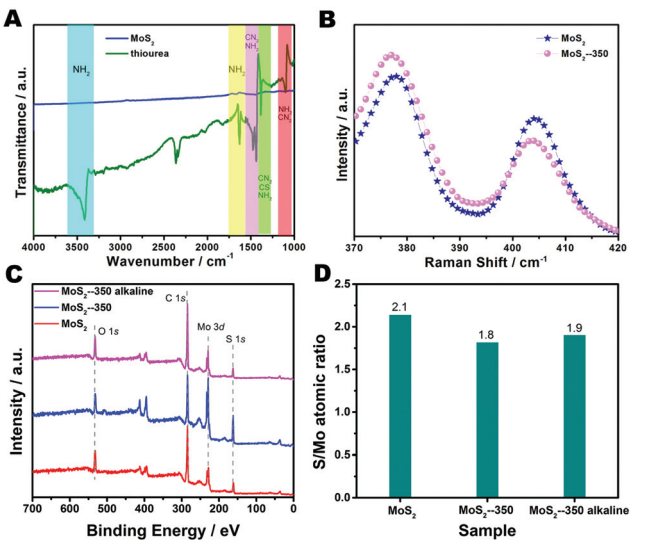

Fig. 2 (A) FTIR spectra of the pristine MoS_2 nanosheets and pure thiourea, (B) Raman, (C) XPS and (D) the atomic ratio between S and Mo for the samples.

X-ray photoelectron spectroscopy (XPS) experiments were carried out to investigate the surface status and composition of the products. As shown in Fig. 2C, most of the Mo signal arose from a 3d peak located at 229 eV, which is characteristic of the +4 oxidation state. Additionally, the 2p peak of sulfur was at 162 eV, corresponding to a −2 valence state.[12] Quantitative analyses showed that the pristine nanosheets had an actual surface composition of $MoS_{2.1}$, which evolved to $MoS_{1.8}$ after treatment at 350 °C (Fig. 2D). The significant composition change could be caused by gradual S vaporization at elevated temperature, which decreased the S content and led to more S defect sites being generated on the nanosheet surfaces, which was in agreement with the Raman results. After the post annealing, some Mo oxide composites were inevitably found at the surface and therefore the MoS_2-350 sample was treated with alkaline solution to dissolve them and expose more inner S (denoted as MoS_2-350 alkaline). As displayed in Fig. 2D, its quantitative composition changed to $MoS_{1.9}$ which further confirmed more fresh active S sites were generated and the effective engineering on its active sites could be explored.

For studying the effect of annealing treatment on the intrinsic HER property of the 2D MoS_2, both the treated and the pristine nanosheets were loaded onto a rotating disk electrode and tested using a three-electrode electrochemical measurement system. 0.5 M H_2SO_4 (aq) was used as the electrolyte, which was purged with Ar for removal of dissolved oxygen prior to any electrochemical test. Fig. 3A and S1A† show the linear sweep voltammetry (LSV) curves, normalized by the electrochemically active surface area (ECSA) and by mass, for the pristine MoS_2 nanosheets and the samples were treated at different temperatures. The ECSA of the MoS_2 was obtained by running cyclic voltammetry (CV) at different scan rates in the double layer potential region (Fig. 3B and C). The flat-line characteristic of the CV curves indicated little occurrence of Faraday reactions, with the collected currents that were primarily caused by the charging/discharging capacitance of the MoS_2. The ECSA of the material could thus be determined by plotting the extracted current difference at a given potential (0.125 V *vs.* RHE) against the potential scan rate (Fig. 3C), since the ECSA value was discovered to be proportional to the double layer capacitance. It needs to be noted that the ECSA of 2D MoS_2 is not equivalent to its surface area. This is because a large part of the surfaces cannot be accessed by electrons, caused by the poor electron conductivity, and are thus electrochemically inactive. It has been reported that even for single layer MoS_2, the bandgap is still as high as 1.9 eV, which suggests poor conductivity unsuitable for electrocatalysis.[33] As a matter of the fact, the measured ECSA of the MoS_2 nanosheets was dramatically smaller than the surface area values projected from the TEM characterization.

The pristine MoS_2 exhibited an onset potential close to −150 mV *vs.* RHE in the acid solution, and an ECSA-specific current density, which represents the intrinsic HER activity of the catalyst, of 10 mA cm^{-2} at −220 mV. For comparison, a big positive shift of about 100 mV in the onset potential was observed when using the MoS_2-150, indicating much improved HER kinetics, which is a result of the higher concentration of active sites present. A current density of 290 mA cm^{-2} was reached at −220 mV, about 30 times more than that for the pristine MoS_2. The MoS_2-350 showed an even higher current density of 440 mA cm^{-2} at that potential and an even more positive onset potential, indicating further improvement of the catalytic property. The MoS_2 after treatment at 550 °C, *i.e.* MoS_2-550, behaved similar to the MoS_2-350 in HER. The mass

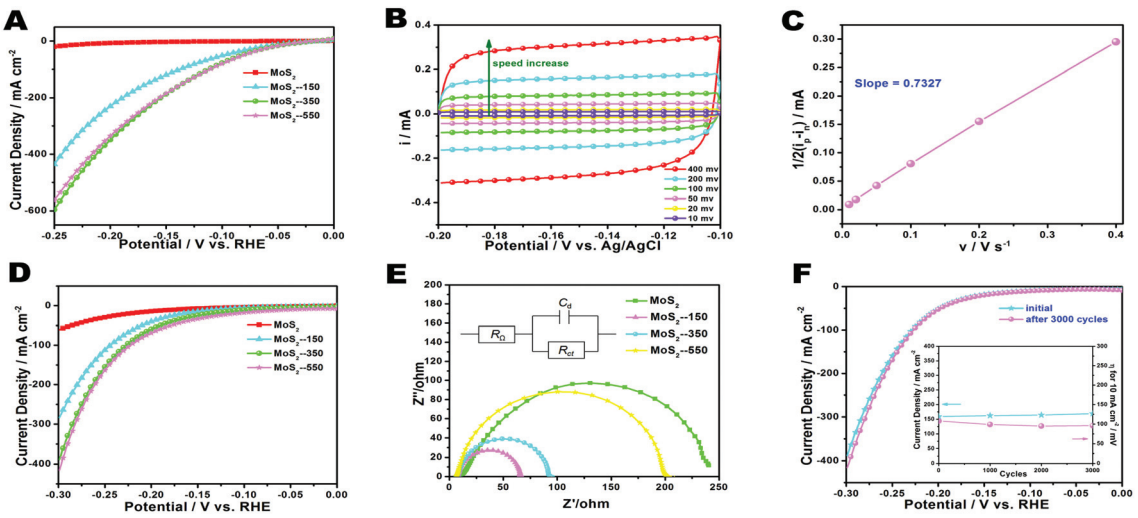

Fig. 3 (A) LSV curves for different MoS_2 nanosheets in 0.5 M H_2SO_4, (B) CV curves obtained for MoS_2 in the double layer potential region and at different scan rates, (C) the current difference between positive scan and negative scan, at 0.125 V *vs.* RHE, as a function of scan rates, (D) LSV curves for all samples in 1 M KOH, (E) Nyquist plots of different samples, with the equivalent circuit inset, and (F) durability measurement of the MoS_2-350. The inset is the current density at −0.25 V *vs.* RHE and a 10 mA cm^{-2} overpotential recorded initially and after every 1000 CV sweeps for the MoS_2-350.

current densities, which is an important measure for practical applications, of the four catalysts were also compared (Fig. S1A†); also a comparison of the onset overpotentials and overpotentials at a 10 mA mg^{-1} current density are listed in Table S1.† All the annealed MoS_2 nanosheets showed higher mass activity than the pristine MoS_2, confirming an effective treatment in improving the catalytic property. It is worth noting that the increase in the mass activity was not as dramatic as in the ECSA-specific activity, which could be caused by an even poorer electron conductivity of the treated nanosheets, making a larger fraction of MoS_2 surface electrons inaccessible and thus electrochemically inactive. Tafel plots obtained from *iR*-corrected polarization curves showed a slope of 54 mV per decade for MoS_2-350, much smaller than that of pristine MoS_2 (Fig. S1B†). This indicates the Volmer–Heyrovsky mechanism for the annealing MoS_2 nanosheets and the chemical desorption process was the rate-limiting step.

The HER property in alkaline electrolyte, which recently has received increasing attention for water splitting, of the treated MoS_2 nanosheets was also studied in 1.0 M KOH aqueous solution. Interestingly, although the proposed mechanisms for HER on MoS_2 are different, the post treatment still led to a dramatic improvement in the reaction kinetics. Fig. 3D and S1C† show ECSA and mass normalized LSV data using the 2D MoS_2. All three treated MoS_2 samples possessed significantly lower onset overpotentials than the pristine MoS_2 nanosheets. Among all, MoS_2-350 and MoS_2-550 exhibited the lowest value of 110 mV. The MoS_2-350 had an extremely large ECSA-specific current density of about 385 mA cm^{-2} at a 300 mV overpotential. This value was about 6.5 times of that for the pristine MoS_2 nanosheets. It is also higher than that for the MoS_2-150 and close to that for the MoS_2-550. For the sake of catalysis, the overpotential is required to achieve 10 mA cm^{-2} current density, which is another pivotal criteria, as it is the approximate current density expected for a solar-to-fuels conversion device with 10% overall efficiency under 1 sun illumination.[34] The MoS_2-350 only needed an overpotential of 95 mV to reach 10 mA cm^{-2}, which is much smaller than the needed 172 mV overpotential when using the pristine MoS_2. The mass activity also followed a similar trend, with the MoS_2-350 and the MoS_2-150 exhibiting the highest mass current density among all four samples. Moreover, the annealing process also dramatically decreased the original Tafel slope to 68 mV per decade (Fig. S1D†). Nyquist plots were acquired and are shown in Fig. 3E. All the annealed MoS_2 exhibited declined charge-transfer resistance (R_{ct}) compared to the pristine nanosheets. The R_{ct} of MoS_2-350 was 87.5 Ω, close to MoS_2-150 (60.3 Ω) and significantly smaller than MoS_2-550 (196.2 Ω), confirming the significant catalytic enhancement. Exchange current densities and TOF values of these samples were also collected and compared with previous reports, as shown in Table S2,† in which MoS_2-350 exhibited the best performance, demonstrating its advanced qualities among the MoS_2 based catalysts.

The boosted HER kinetics of the annealing 2D MoS_2 nanosheets in both acidic and alkaline electrolytes could be attributed to the generation of more fresh active sites. As has been discussed above, the treatment could activate the ultrathin MoS_2 nanosheets and result in gradual loss of surface edge S atoms, which helps to create more in-plane open active edges and is confirmed by the Raman and XPS experiments. On the other side, the electron conductivity of the MoS_2 nanosheets decreased with the treatment temperature, which was revealed by increasing the differences between the measured ECSA values and the real surface area values, and caused more fraction of surface sites to be electrochemically inactive. The two factors counterplay with each other, leading to MoS_2 annealed at 350 °C possessing the most optimal composition and thus the highest mass activity.

Durability is another important criterion to evaluate an electrocatalyst besides the HER activity. Continuous CV scans at a 50 mV s^{-1} rate in the potential window between −300 and 0 mV *vs.* RHE were carried out to investigate long term durability of the MoS_2-350. Interestingly, there was a negligible difference between the LSV curves measured initially and after 3000 CV cycles, illustrating excellent durability of the catalyst in the operational potential range (Fig. 3F). As shown in the corresponding inset diagram, from the current density recorded at η = 250 mV and the overpotential values recorded at 10 mA cm^{-2}, it can be observed that the MoS_2-350 showed only a slight change in the activity during the durability test. Thus, it can be concluded that the MoS_2-350 nanosheets possessed both superior HER activity and excellent durability in alkaline electrolyte, which makes it a valuable and promising catalyst for practical applications.

In summary, we have created more fresh active sites on the synthesized 2D MoS_2 nanosheets and thus improved the intrinsic HER property. During the simple annealing treatment process, the old edge S atoms were vaporized or removed and more fresh active edges were generated and exposed. The active sites were controllable and MoS_2-350 exhibited the largest activity improvement compared to the pristine MoS_2 nanosheets in both acidic and alkaline electrolytes. It showed both ECSA and mass normalized activity enhancement, as well as good durability, confirming effectiveness of the post treatment for the active sites engineering and providing a new strategy for designing HER catalysts.

This work was supported by the University of Akron start-up fund (Z. P.) and by the National Natural Science Foundation of China (51602116) (to X. K.). TEM data were obtained at the (cryo)TEM facility at the Liquid Crystal Institute, Kent State University, supported by the Ohio Research Scholars Program Research Cluster on Surfaces in Advanced Materials.

Notes and references

1 M. S. Dresselhaus and I. L. Thomas, *Nature*, 2001, **414**, 332–337.
2 J. A. Turner, *Science*, 2004, **305**, 972–974.
3 S. Chen, Y. Qi, T. Hisatomi, Q. Ding, T. Asai, Z. Li, S. S. K. Ma, F. Zhang, K. Domen and C. Li, *Angew. Chem., Int. Ed.*, 2015, **54**, 8498–8501.

4 Y. Zhang, J. Zhang, Q. Xu, S. Yan, S. Zhao, G. Luo and C. Li, *Mater. Res. Bull.*, 2014, **53**, 107–115.
5 C. Kong, S. Min and G. Lu, *Chem. Commun.*, 2014, **50**, 9281–9283.
6 P. Chen, K. Xu, Y. Tong, X. Li, S. Tao, Z. Fang, W. Chu, X. Wu and C. Wu, *Inorg. Chem. Front.*, 2016, **3**, 236–242.
7 M. S. Faber, R. Dziedzic, M. A. Lukowski, N. S. Kaiser, Q. Ding and S. Jin, *J. Am. Chem. Soc.*, 2014, **136**, 10053–10061.
8 D. Voiry, H. Yamaguchi, J. Li, R. Silva, D. C. B. Alves, T. Fujita, M. Chen, T. Asefa, V. B. Shenoy, G. Eda and M. Chhowalla, *Nat. Mater.*, 2013, **12**, 850–855.
9 S. Jin, X. Wang, X. Wang, M. Ju, S. Shen, W. Liang, Y. Zhao, Z. Feng, H. Y. Playford, R. I. Walton and C. Li, *J. Phys. Chem. C*, 2015, **119**, 18221–18228.
10 K. Xu, P. Chen, X. Li, Y. Tong, H. Ding, X. Wu, W. Chu, Z. Peng, C. Wu and Y. Xie, *J. Am. Chem. Soc.*, 2015, **137**, 4119–4125.
11 H. Vrubel and X. Hu, *Angew. Chem., Int. Ed.*, 2012, **51**, 12703–12706.
12 J. Kibsgaard, Z. Chen, B. N. Reinecke and T. F. Jaramillo, *Nat. Mater.*, 2012, **11**, 963–969.
13 A. B. Laursen, S. Kegnaes, S. Dahl and I. Chorkendorff, *Energy Environ. Sci.*, 2012, **5**, 5577–5591.
14 H. Vrubel, D. Merki and X. Hu, *Energy Environ. Sci.*, 2012, **5**, 6136–6144.
15 Y. Li, H. Wang, L. Xie, Y. Liang, G. Hong and H. Dai, *J. Am. Chem. Soc.*, 2011, **133**, 7296–7299.
16 Y. Huang, R. J. Nielsen, W. A. Goddard and M. P. Soriaga, *J. Am. Chem. Soc.*, 2015, **137**, 6692–6698.
17 X. Y. Yu, H. Hu, Y. Wang, H. Chen and X. W. Lou, *Angew. Chem., Int. Ed.*, 2015, **54**, 7395–7398.
18 J. Deng, H. Li, J. Xiao, Y. Tu, D. Deng, H. Yang, H. Tian, J. Li, P. Ren and X. Bao, *Energy Environ. Sci.*, 2015, **8**, 1594–1601.
19 X. Zhang, F. Meng, S. Mao, Q. Ding, M. J. Shearer, M. S. Faber, J. Chen, R. J. Hamers and S. Jin, *Energy Environ. Sci.*, 2015, **8**, 862–868.
20 D. J. Li, U. N. Maiti, J. Lim, D. S. Choi, W. J. Lee, Y. Oh, G. Y. Lee and S. O. Kim, *Nano Lett.*, 2014, **14**, 1228–1233.
21 J. Xie, H. Zhang, S. Li, R. Wang, X. Sun, M. Zhou, J. Zhou, X. W. Lou and Y. Xie, *Adv. Mater.*, 2013, **25**, 5807–5813.
22 X. K. Kong, Z. Y. Sun, M. Chen, C. L. Chen and Q. W. Chen, *Energy Environ. Sci.*, 2013, **6**, 3260–3266.
23 V. K. Sangwan, D. Jariwala, I. S. Kim, K.-S. Chen, T. J. Marks, L. J. Lauhon and M. C. Hersam, *Nat. Nanotechnol.*, 2015, **10**, 403–406.
24 T. F. Jaramillo, K. P. Jørgensen, J. Bonde, J. H. Nielsen, S. Horch and I. Chorkendorff, *Science*, 2007, **317**, 100–102.
25 D. Kong, H. Wang, J. J. Cha, M. Pasta, K. J. Koski, J. Yao and Y. Cui, *Nano Lett.*, 2013, **13**, 1341–1347.
26 H. Wang, Z. Lu, S. Xu, D. Kong, J. J. Cha, G. Zheng, P. C. Hsu, K. Yan, D. Bradshaw, F. B. Prinz and Y. Cui, *Proc. Natl. Acad. Sci.U. S. A.*, 2013, **110**, 19701–19706.
27 H. I. Karunadasa, E. Montalvo, Y. Sun, M. Majda, J. R. Long and C. J. Chang, *Science*, 2012, **335**, 698–702.
28 J. Kibsgaard, T. F. Jaramillo and F. Besenbacher, *Nat. Chem.*, 2014, **6**, 248–253.
29 Y. Sun, S. Gao, F. Lei and Y. Xie, *Chem. Soc. Rev.*, 2015, **44**, 623–636.
30 Y. Guo, K. Xu, C. Wu, J. Zhao and Y. Xie, *Chem. Soc. Rev.*, 2015, **44**, 637–646.
31 M. Yan, K. Liu and Z. Jiang, *J. Electroanal. Chem.*, 1996, **408**, 225–229.
32 K. G. Zhou, F. Withers, Y. Cao, S. Hu, G. Yu and C. Casiraghi, *ACS Nano*, 2014, **8**, 9914–9924.
33 A. Splendiani, L. Sun, Y. Zhang, T. Li, J. Kim, C. Y. Chim, G. Galli and F. Wang, *Nano Lett.*, 2010, **10**, 1271–1275.
34 C. C. L. McCrory, S. Jung, I. M. Ferrer, S. M. Chatman, J. C. Peters and T. F. Jaramillo, *J. Am. Chem. Soc.*, 2015, **137**, 4347–4357.

